Phosphorylation of a *Toxoplasma gondii* tyrosine transporter by calcium-dependent kinase 3 is important for parasite fitness.

Short Title: Phosphorylation of a tyrosine transporter in *Toxoplasma gondii*

Bethan A. Wallbank[1], Caia S. Dominicus[1¶], Malgorzata Broncel[1¶], Nathalie Legrave[2], James I. MacRae[2], Henry M. Staines[3] and Moritz Treeck[1*]

[1] Signalling in Apicomplexan Parasites Laboratory, The Francis Crick Institute, London, United Kingdom

[2] Metabolomics Science Technology Platform, The Francis Crick Institute, London, United Kingdom

[3] St George's, University of London, Institute of Infection and Immunity, London, United Kingdom

* Corresponding author treeckm@crick.ac.uk (MT)

¶These authors contributed equally to this work

Abstract

Toxoplasma gondii parasites rapidly exit their host cell when exposed to calcium ionophores. The calcium-dependent protein kinase 3 (*Tg*CDPK3) was previously identified as a key mediator in this process, as *Tg*CDPK3 knockout (Δ*cdpk3*) parasites fail to egress in a timely manner. Phosphoproteomic analysis comparing WT with Δ*cdpk3* parasites revealed changes in the *Tg*CDPK3-dependent phosphoproteome that included proteins important for regulating motility, but also metabolic enzymes, indicating that *Tg*CDPK3 controls processes beyond egress. Here we have investigated a predicted direct target of *Tg*CDPK3, a putative transporter of the major facilitator superfamily (MFS) and show that it is rapidly phosphorylated after induction of calcium signalling. Conditional knockout (KO) of the transporter reveals an essential role in the lytic cycle during intracellular growth with a transcriptome signature of amino acid-starved parasites. Using a combination of metabolomics and heterologous expression, we confirmed a primary role in tyrosine import. Complementation with phosphorylation site mutants shows that phosphorylation of serine 56 (S56) by *Tg*CDPK3 gives the parasites a growth benefit in competition assays. Collectively, these findings validate an important, albeit non-essential role for *Tg*CDPK3 in the regulation of metabolic processes, in addition to motility.

Author summary

Toxoplasma gondii is an obligate intracellular parasite. To survive and spread throughout the host it must repeatedly infect, replicate within and exit, host cells. These recurring cycles of infection and egress rely on signalling pathways that

allow the parasites to sense and respond rapidly to their environment. While some key kinases and secondary messengers within these pathways have been identified, functional analysis of non-kinases has been very limited. This is especially true for candidates that are not predicted to play a role in active motility or are not known to function in established signalling pathways. Here we have followed up on an unexpected target of the *T. gondii* calcium-dependent kinase 3 (*Tg*CDPK3), a plant-like calcium dependent kinase, that was previously shown to play an important role in calcium-mediated exit from the host cell. We show that, in addition to controlling motility of the parasite (as previously shown), *Tg*CDPK3 phosphorylates an essential tyrosine transporter in the plasma membrane. Mutational analysis of the phosphorylation sites demonstrates an important role in maintaining parasite fitness, thus demonstrating that *Tg*CDPK3 plays a pleiotropic role in controlling both egress and metabolism.

Introduction

The fast growing tachyzoite stage of the protozoan parasite *Toxoplasma gondii* requires cycles of host cell invasion, replication, and lysis for its successful proliferation within the host. Each step of this lytic cycle involves tightly regulated signalling pathways, the intricacies of which remain largely unknown. Paramount to parasite survival is the ability to sense and respond to changes in the environment for which the divalent calcium ion (Ca^{2+}) acts as an important secondary messenger (1). Changes in free intracellular $[Ca^{2+}]_i$ levels, via release of Ca^{2+} from organellar Ca^{2+} stores, can be induced by the addition of Ca^{2+} ionophores, such as A23187 or phosphodiesterase inhibitors (2,3). Ca^{2+} flux regulates key processes including secretion of micronemes

prior to host cell entry (4), parasite motility (5), and host cell egress (6) and invasion (7). Inversely, these processes can all be inhibited by Ca^{2+} immobilisers or chelators, such as BAPTA-AM (5,8–10). Ca^{2+} release leads to the activation of Ca^{2+} binding proteins such as calmodulins, calcineurin B-like kinases and calcium-dependent protein kinases (CDPKs). *T. gondii* calcium-dependent protein kinase 3 (*Tg*CDPK3), for example, has been implicated in the regulation of ionophore induced egress, IIE (i.e. the rapid exit of tachyzoites from a host cell on addition of ionophore) and ionophore induced death, IID (i.e. the loss of infectivity of EC parasites after prolonged exposure to ionophore) (9). *TgCDPK3* KO (Δ*cdpk3*) (11), mutants (9), and chemically inhibited *Tg*CDPK3 lines (12) all show a deficiency in IIE and IID. *Tg*CDPK3 is a serine/threonine kinase belonging to a large family of CDPKs also found in plants and ciliates, but absent in humans. It is anchored to the parasite plasma membrane, via N-terminal myristoylation and palmitoylation motifs (11–13), facing the lumen of the parasite. Like all CDPKs, *Tg*CDPK3 possesses a C-terminal calmodulin-like domain consisting of 4 EF hands, known as the CDPK activation domain, as well as upstream autoinhibitory and catalytic domains (14). Binding of Ca^{2+} to the EF hands causes a structural rearrangement that frees up the active site of the kinase domain, allowing for substrate phosphorylation (15,16). A quantitative phosphoproteome study revealed 156 phosphorylation sites that are differentially phosphorylated between WT and *Tg*CDPK3 mutant parasites (17). The *Tg*CDPK3-dependent phosphoproteome includes phosphorylation sites on proteins involved in parasite motility, such as the cyclase-associated protein and myosin A (Myo A), but also, and perhaps surprisingly, those involved in metabolic processes such as the α-ketoacid dehydrogenase (BCKDH) subunit, E1α, required for the breakdown of branched-chain amino acids (BCAAs) and conversion of pyruvate to the TCA driver acetyl-CoA (18). The link to proteins not

obviously involved in egress and motility, as well as changes in the phosphoproteome regardless of the presence of ionophore, suggests that *Tg*CDPK3 function extends beyond egress.

The phosphorylation site that appeared to have one of the most marked reductions in phosphorylation state in *Tg*CDPK3 mutants compared to WT parasites (17), is situated within a putative transporter of the MFS family (TGGT1_257530, named ApiAT5-3 as per (19)) that has moderate homology to a BCAA transporter. Given the additional evidence from the phosphoproteomic dataset that *Tg*CDPK3 putatively regulates BCAA catabolism via BCKDH, we hypothesised that *Tg*CDPK3 might be involved in BCAA uptake and metabolism via phosphorylation of ApiAT5-3 in addition to regulating motility. Here, we have assessed the function of ApiAT5-3 and the role of *Tg*CDPK3-mediated phosphorylation. We show that ApiAT5-3 is rapidly phosphorylated at serine 56 (S56) during the first minute of induced egress. Using a conditional KO approach, we show that ApiAT5-3 is essential, and that deletion leads to a delayed death phenotype that is accompanied by a transcriptional response relating to translational stress. In growth competition assays performed with parasite lines that rely on phosphomutants or phosphomimetics, we show that phosphorylation of S56 appears to be important, but not essential, for parasite fitness. Finally, using a combination of metabolic analysis and heterologous expression in *Xenopus laevis* oocytes we confirm that ApiAT5-3 transports tyrosine but has only limited capacity to transport BCAAs. This data confirms that *Tg*CDPK3 phosphorylates several targets in its vicinity, controlling diverse processes at the plasma membrane and thus contributing to a range of biological processes in the parasite.

Results

ApiAT5-3 is located at the parasite periphery and phosphorylated during ionophore induced egress in a *Tg*CDPK3-dependent manner.

ApiAT5-3 was previously identified to be phosphorylated at Serine 56 in a *Tg*CDPK3-dependent manner (17). BLAST analysis using the Transporter Classification Database (http://www.tcdb.org/) predicts that ApiAT5-3 possesses a modest level of homology to a BCAA transporter. This was interesting, as deletion of *TgCDPK3* was previously shown to lead to upregulation of the BCKDH complex (17), involved in BCAA catabolism. This indicated that *Tg*CDPK3 may directly control BCAA transport by phosphorylating ApiAT5-3.

Topology prediction (https://embnet.vital-it.ch/software/TMPRED_form.html (20)) places the N-terminal regions of ApiAT5-3 at the luminal side of the parasite, potentially allowing for direct interaction with *Tg*CDPK3, which also localises to the plasma membrane (Fig. 1A). ApiAT5-3 contains several phosphorylation sites at its N-terminus, of which S56 was the only one previously identified as being *Tg*CDPK3-dependent (Fig. 1B, upper panel). It is entirely plausible, however, that kinases other than *Tg*CDPK3 act during egress to phosphorylate additional residues on the ApiAT5-3 N-terminus. To investigate this, we queried a dataset recently generated in our laboratory in which we have quantified, using tandem-mass-tag technology (21), phosphorylation site abundance on *T. gondii* proteins across 4 time points (0, 15, 30 and 60 s) following ionophore-treatment (Caia Dominicus, in preparation). From the ~850 phosphorylation sites that are phosphorylated or de-phosphorylated during egress, we identified S56 of ApiAT5-3 as increasingly phosphorylated over time (Fig. 1B, lower panel). We also

identified several proteins already known to be more phosphorylated in response to Ca^{2+} signalling including MyoA, Myosin F and DrpB (17,22,23). None of the other phosphorylation sites on the ApiAT5-3 N-terminus increased in phosphorylation state prior to, or during egress. However, S14 of ApiAT5-3 was dephosphorylated during ionophore-treatment. Collectively these data indicate that S56 is phosphorylated in a *Tg*CDPK3-dependent manner upon Ca^{2+} stimulation, and that a phosphatase is acting on S14 during the same period, while the other phosphorylation sites appear unaffected.

To localise ApiAT5-3 in *T. gondii* parasites we generated an RH parasite line (ApiAT5-3::HA) that expressed a C-terminally HA-epitope tagged version of ApiAT5-3 under control of its endogenous promotor (i.e. 1000 bp upstream of the start ATG). Western Blotting confirmed expression of a 42 KDa protein close to the predicted size (56 KDa) (Fig. 1C) and immunofluorescence assays (IFA) showed ApiAT5-3 predominantly at the periphery of the parasite (Fig. 1D). No ApiAT5-3::HA could be detected in nascent daughter cells, a hallmark of most inner membrane complex proteins. Together, these data suggest that ApiAT5-3 localises, like *Tg*CDPK3, to the plasma membrane, and thus, could be a *bona fide* target of *Tg*CDPK3 *in vivo*.

apiAT5-3 deletion causes delayed parasite death

ApiAT5-3 depletion is predicted to have a high fitness cost (Toxo DB 7.1 (24)). Accordingly, we generated a conditional KO using the dimerisable cre recombinase (DiCre) strategy. We replaced the endogenous copy of *apiAT5-3* with a recodonised version in RH $\Delta ku80^{DiCre}$ parasites, by double homologous

169 recombination, using a double-guide strategy (25) (Fig. 2A). We initially placed a
170 loxP site adjacent to the Kozac sequence of ApiAT5-3 but were unable to obtain
171 correct integration. We hypothesised that the loxP sequence might be interfering
172 with promotor elements and moved it 100 and 200 bp upstream of the predicted
173 start ATG, respectively. Both of these constructs correctly integrated into the
174 genome. Subsequent analyses were performed with the resulting ApiAT5-3_loxP,
175 with the loxP at ATG -100bp. Integration was confirmed by PCR amplification (Fig.
176 2B, left panel). To test whether ApiAT5-3 is an essential gene we treated parasites
177 for 4h with either rapamycin (RAP) or DMSO. PCR analysis showed a near
178 complete excision of the floxed gene (Fig. 2B, right panel). Correct excision of the
179 ApiAT5-3 open reading frame resulted in YFP positive parasites that could be
180 readily distinguished from WT by microscopy (Fig. 2C). Upon performing plaque
181 assays it became evident that RAP, but not DMSO-treatment, resulted in a
182 complete block in plaque formation (Fig. 2D). A small number (<0.5%) of plaques
183 could be identified in RAP-treated cultures, however, parasites contained in these
184 plaques where YFP(-), indicating that they arose from non-excised parasites (data
185 not shown). Over time these non-excised parasites within the RAP-treated
186 population outgrew the KOs (Fig. S1), further reinforcing the fact that ApiAT5-3 is
187 essential for parasite survival. These non-excising parasites (termed ApiAT5-
188 3_loxP^{dDiCre}), which presumably possess a non-functioning diCre recombinase,
189 were isolated and used as controls for subsequent experiments, as detailed below.
190
191 To visualise at which time points ApiAT5-3 is important, we followed replication
192 of live RAP-treated ApiAT5-3_loxP parasites over 3 lytic cycles, where each lytic
193 cycle is defined as growth over 36 hrs, before passage into a fresh culture dish

194 containing host cells. This analysis revealed that in the first cycle, RAP-treated
195 (*apiAT5-3* KO) parasite numbers and replication rate remained comparable to
196 DMSO-treated (WT) parasites (Fig. 2E). However, by 36 hrs into the second
197 replicative cycle there was a 60.7% decrease in the number of vacuoles with more
198 than 16 parasites compared to the DMSO control. By the end of the 3rd cycle the
199 *apiAT5-3* KO parasites consisted largely of 2 or fewer parasites/vacuole, even
200 after the WT had successfully egressed (48 hrs into cycle). To better identify
201 phenotypic consequences of *apiAT5-3* deletion, we followed replication over time
202 using live-video microscopy. We started recording 29 hrs into the third lytic cycle
203 post RAP-treatment, by which time *apiAT5-3* KO parasites display a marked
204 growth defect. To facilitate a more accurate comparison between *apiAT5-3* KO and
205 WT parasites, tdTomato expressing RH parasites (RH Tom) were spiked into the
206 imaging wells at a 1:1 ratio. These analyses revealed that *apiAT5-3* KO does not
207 lead to early egress or an inability to invade, but rather a lack of replication, often
208 with the ability to undergo a first division, but failing to go beyond 2
209 parasites/vacuole (Fig. 2F, Movies S1A and B).
210 As we showed that ApiAT5-3 is phosphorylated directly after ionophore-
211 treatment (Fig. 1B), we postulated that it may be required for ionophore induced
212 egress. To assess this, we performed egress assays of the DMSO- and RAP-treated
213 lines in the presence of 8 µM Ca^{2+} ionophore. However, there was no significant
214 difference between the KO and WT (Fig. 2G) suggesting that phosphorylation of
215 ApiAT5-3, in response to elevated Ca^{2+} levels, plays a role in processes other than
216 egress.
217

***apiAT5-3* KO parasites display a transcriptional response related to amino acid starvation**

Deletion of a transporter may lead to up-regulation of alternative transporters or may manifest as a stress response that carries a detectable signature. To investigate this, we measured transcript levels using RNAseq, comparing RAP-treated ApiAT5-3_loxP with ApiAT5-3_loxP^{dDiCre} parasites, which, as mentioned previously, do not excise the endogenous locus, even when treated with RAP. RNA was isolated in biological triplicate at 4 hrs post RAP-treatment, the time point at which we did not expect to see major changes in the transcriptome, and 60 hrs post treatment, by which time point the RAP-treated ApiAT5-3_loxP parasites are still viable but start to display a growth defect. Indeed, at 4 hrs transcripts from the *apiAT5-3* gene were only slightly reduced in the RAP-treated ApiAT5-3_loxP parasites compared to the RAP-treated ApiAT5-3_loxP^{dDiCre} parasites (17.1%). In contrast, at 60 hrs post RAP-treatment, a 64.7% reduction was observed (Fig. 3A). Unexpectedly, only 435 transcripts showed a statistically significant differential expression between the WT and *apiAT5-3* KO parasites at the 60 hrs time point, compared to the 4 hrs time point, indicating a modest transcriptional response to *apiAT5-3* deletion (Fig. 3B). GO-term analysis of the differentially transcribed genes showed most enrichment (5.41-fold) for genes important for translation. Among this enriched group, these genes encode almost exclusively genes for ribosomal proteins (Fig. 3C, Table S3). No single transporter was specifically up-regulated, indicating that there is no rapid transcriptional compensation when *apiAT5-3* is deleted.

242 Collectively these data show that ApiAT5-3 is an essential protein that is required
243 for intracellular replication. Its depletion leads to a complete arrest in growth
244 which is not accompanied by a substantial stress response, but rather modest
245 signs of translational stress.
246

247 **Mutation of S56 to alanine, but not a phosphomimetic leads to a reduction in fitness.**
248 Having established that ApiAT5-3 is essential for the lytic cycle, we next sought to
249 examine the role of *Tg*CDPK3-mediated phosphorylation in ApiAT5-3 function. To
250 do this, we complemented ApiAT5-3_loxP parasites with either WT ApiAT5-3, or
251 variants where S56 is mutated to alanine (S56A) or to aspartic acid (S56D). To
252 prevent possible differences in growth between the parasite lines due to
253 differential expression of the complementation constructs, we inserted each into
254 the *uprt* locus by double homologous recombination, under control of the
255 endogenous promoter (Fig. 4A). Complementation into the *uprt* locus was verified
256 by PCR (Fig. 4B). The complementation constructs also carried a C-terminal HA
257 epitope tag to verify correct trafficking to the plasma membrane.
258 Immunofluorescence displayed correct trafficking in all variants (Fig. 4C).
259 To compare fitness between the WT, the phosphomimetic (S56D), and the
260 phosphomutant (S56A) complemented lines in the absence of *apiAT5-3*, we
261 deleted the endogenous copy using RAP-treatment. This results in parasite strains
262 that solely rely on the complemented copy of the gene. We confirmed correct
263 excision of *apiAT5-3* by virtue of YFP expression post RAP-treatment, and PCR
264 analysis (Fig. 4C, Fig. S2A). RAP-treated parasite lines were viable and allowed us
265 to isolate clones by limiting dilution, all of which restored growth in plaque assays
266 (Fig. S2B). This shows that i) complementation of *apiAT5-3* by expression at the

267 *uprt* locus fully restores ApiAT5-3 function and ii) that neither the introduction of
268 phosphomimetics nor phosphomutants of S56 are lethal to parasite growth.
269 This is not surprising as deletion of *Tg*CDPK3, the kinase putatively responsible
270 for ApiAT5-3 phosphorylation during egress, does not lead to a severe growth
271 phenotype. Accordingly, phosphomutants would not be expected to display
272 drastic differences in growth. We therefore performed competition assays in
273 which we compared growth of YFP expressing complementation lines that fully
274 rely on the complementation variant for growth (Δ*apiAT5-3*$^{\text{ApiAT5-3/S56A/S56D}}$)
275 mixed in a 1:1 ratio with their non-excised, colourless counterpart (ApiAT5-
276 3$^{\text{ApiAT5-3/S56A/S56D}}$). Using the ratio of 4',6-diamidino-2-phenylindole (DAPI) stained
277 parasites (DAPI labels the DNA of all parasites) and YFP expressing parasites (YFP
278 is expressed only in the complementation lines) we followed growth over 14 days
279 in biological triplicates. While Δ*apiAT5-3*$^{\text{ApiAT5-3}}$ parasites showed no difference in
280 growth compared to their WT control, Δ*apiAT5-3*$^{\text{ApiAT5-3\_S56A}}$ was reduced by
281 84.0% after 14 days (Fig. 4D). Strikingly, Δ*apiAT5-3*$^{\text{ApiAT5-3\_S56D}}$ was not
282 outcompeted and grew at similar levels to the WT control.
283 Collectively these data indicate that phosphorylation of S56 while not essential, is
284 important for intracellular growth.
285

286 **ApiAT5-3 is a primary transporter of tyrosine, but not branched chain amino acids**
287 The predicted homology of ApiAT5-3 to a BCAA transporter and the profound up-
288 regulation of the BCKDH complex in Δ*cdpk3* parasites suggested a direct role for
289 ApiAT5-3 in BCAA transport. To test this, we expressed *apiAT5-3* in the
290 heterologous expression system, *X. laevis* oocytes. Concurrently with our study,
291 data were presented that ApiAT5-3 may be a tyrosine transporter (Giel van

292 Dooren, personal communication and pre-published in BioRx (19)). We therefore
293 tested BCAA import and replicated the tyrosine uptake capacity of ApiAT5-3 in
294 oocytes expressing WT ApiAT5-3 (Fig. 5A). Measuring unidirectional influx, we
295 observed a significant (4.0-fold) increase in the uptake of ^{14}C-tyrosine into
296 ApiAT5-3-expressing oocytes compared to either water-injected or uninjected
297 control oocytes under the conditions tested, consistent with results from (19). We
298 also observed moderate ApiAT5-3-dependent phenylalanine influx, but not for the
299 BCAA valine (Fig. S3A), suggesting that, while ApiAT5-3 is capable of tyrosine
300 transport, it is unlikely to be a major BCAA transporter.

301 To verify the role of ApiAT5-3 in tyrosine transport in our conditional KO
302 parasites, we measured intracellular ^{13}C-tyrosine levels in RAP-treated Δ*apiAT5-*
303 *3*$^{\text{ApiAT5-3}}$ (WT) and ApiAT5-3_loxP (KO) parasites (74 hrs post excision), after 1 hr
304 in the presence of growth media containing ^{13}C-tyrosine. In an analogous manner,
305 we also measured ^{13}C-isoleucine uptake in order to verify if ApiAT5-3 is also a
306 BCAA transporter. Δ*apiAT5-3*$^{\text{ApiAT5-3}}$ was used instead of DMSO-treated ApiAT5-
307 3_loxP to control for any potential effects of rapamycin on parasite metabolism.
308 This analysis verified a reduction of ^{13}C-labelled tyrosine uptake (40.5%
309 compared to *ΔapiAT5-3*$^{\text{ApiAT5-3}}$), but not isoleucine uptake (4.3% compared to
310 *ΔapiAT5-3*$^{\text{ApiAT5-3}}$) (Fig. 5B). We also measured the intracellular abundance of all
311 detectable amino acids when labelling with ^{13}C-tyrosine. We observed a reduction
312 of intracellular tyrosine abundance (63.2%) in the Δ*apiAT5-3*$^{\text{ApiAT5-3}}$ cells (as
313 expected), but not phenylalanine which was slightly increased in relative
314 abundance (17.45%), suggesting that while ApiAT5-3 is able to transport
315 phenylalanine in oocytes, it is not the major phenylalanine transporter in *T. gondii*

316 (Fig. S3B). It is important to note that our metabolome analysis was performed at
317 the end of cycle 2 after RAP-treatment, when *ΔapiAT5-3*$^{ApiAT5-3}$ parasites are still
318 viable but start to display a reduction of growth (Fig. 2e). Therefore, we predict
319 that low levels of ApiAT5-3$^{ApiAT5-3}$ present at this stage are responsible for the
320 residual transport of tyrosine. Interestingly, we also observed a reduction in
321 intracellular aspartate (38.5%) and glycine (28.3%) in Δ*apiAT5-3*$^{ApiAT5-3}$ cells (Fig.
322 S3B). Since *T. gondii* is not known to be auxotrophic for these amino acids we
323 reasoned that the observed death phenotype is unlikely caused by a defect in
324 glycine or aspartate import, and instead focussed our subsequent analysis on
325 tyrosine. We also observed an increase in the abundance of glutamine, valine,
326 isoleucine and proline, indicating potential wider metabolic effects.
327
328 To test whether exogenous tyrosine can complement the loss of ApiAT5-3 we
329 grew parasites in media with 5× the normal amount of tyrosine (2 mM). Despite
330 various attempts to restore normal growth or generate Δ*apiAT5-3* clonal lines, we
331 could not obtain viable parasites in high tyrosine (Fig. 5C). In other organisms,
332 phenylalanine can be converted into tyrosine. Therefore, we tested whether
333 phenylalanine supplementation (2 mM) can rescue the growth phenotype of
334 *apiAT5-3* KO parasites. No growth rescue could be observed (data not shown).
335 Together, these results suggest that ApiAT5-3 is the only transporter of tyrosine
336 in *T. gondii* and that phenylalanine cannot be readily converted into tyrosine in *T.*
337 *gondii* parasites.
338
339 To identify whether differences in phosphorylation state of ApiAT5-3 affected
340 tyrosine transport, we performed isotopic tyrosine labelling of extracellular

341 parasites using the Δ*apiAT5-3*$^{\text{ApiAT5-3\_S56A}}$ and Δ*apiAT5-3*$^{\text{ApiAT5-3\_S56D}}$
342 phosphomutant strains. No significant differences could be observed in these
343 assays indicating that, if tyrosine import is affected, differences may be obstructed
344 by the intrinsic variability of the assay (data not shown).
345 The fitness phenotype of mutating S56 to alanine is modest in a single lytic cycle
346 and thus not predicted to have substantial impact on the import of tyrosine.
347 Because we could not measure differences in tyrosine import in our
348 phosphorylation site mutants we turned to heterologous assays where we
349 expressed ApiAT5-3 WT, S56A and S56D in *X. laevis* oocytes and tested tyrosine
350 uptake. Although there was a trend towards a reduction in tyrosine uptake in the
351 S56A expressing oocytes (average 19.5% reduction in S56A relative to WT
352 ApiAT5-3 expressing oocytes), this difference was not statistically significant (Fig.
353 5D). The S56D expressing oocytes display a marginal increase in tyrosine uptake
354 of 14.0%, that again was not statistically significant.
355 Collectively these data show that conditional deletion of ApiAT5-3 causes a lethal
356 reduction in tyrosine import that cannot be compensated for by amino acid
357 supplementation. We also show that while phosphorylation of ApiAT5-3 at S56 is
358 not required for tyrosine transport, mutating that site to alanine does lead to a
359 subtle decrease in tyrosine transport in a heterologous assay.
360

361 ## Discussion

362 *Tg*CDPK3 has previously been implicated in controlling distinct biological
363 processes such as gliding motility and metabolism. How these are linked, however,
364 has been unclear. Mutants that display only IIE and IID phenotypes have been

365 identified (9,26), arguing that *Tg*CDPK3 may be an upstream regulator of both
366 processes. Here we show that upon activation by the Ca^{2+} ionophore A23187,
367 *Tg*CDPK3 leads to an increase in ApiAT5-3 phosphorylation at S56. This occurs at
368 the same time, and to a similar intensity, as other previously identified targets of
369 *Tg*CDPK3 (e.g. serine 21/22 of MyoA) and other kinases involved in signalling (e.g.
370 *Tg*CDPK1). MyoA and ApiAT5-3 are both located at, or close to, the plasma
371 membrane. It is conceivable that, upon activation, *Tg*CDPK3 phosphorylates
372 proteins at the plasma membrane, some of which are important for motility and
373 others (e.g. transporters) that prepare the parasite for the extracellular milieu. In
374 this study we have identified a function for the phosphorylation of S56, which
375 becomes rapidly phosphorylated prior to egress in a *Tg*CDPK3-dependent
376 manner. Interestingly, ApiAT5-3 possesses several other phosphorylation sites in
377 its N-terminus, aside from S56, that either do not change in phosphorylation state
378 or, in the case of S14, appear dephosphorylated during induced Ca^{2+} signalling.
379 How S14 dephosphorylation and S56 phosphorylation are controlling ApiAT5-3
380 function requires further investigation, however it is evident that mutating S56 to
381 a non-phosphorylatable residue substantially reduces parasite fitness.
382 Phosphorylation of transporters has been shown to regulate affinity, specificity
383 and flux of cargo (27–32). Accordingly, the observed fitness cost in S56A mutants
384 could be indicative of a reduction in tyrosine import, for which the parasite is
385 auxotrophic (33).
386 While we observed a clear role for ApiAT5-3 in tyrosine transport, expression of
387 the ApiAT5_S56A phosphomutant only led to a modest reduction in tyrosine
388 import in oocytes, which was not statistically significant. One explanation could
389 be that the effect on tyrosine import is beyond the limit of detection in our assays.

We observed an 84.0% reduction in growth of Δ*apiAT5-3*$^{\text{ApiAT5-3\_S56A}}$ mutants compared to WT parasites over 14 days. This translates into a reduced replication rate of ~6.74% per 24 hrs. Tyrosine uptake assays in oocytes, as well as in extracellular parasites are, for reasons of cell viability, performed in <1 hr, and may therefore not pick up the subtle differences predicted to occur if tyrosine is the only limiting factor in these assays. Furthermore, as indicated above, ApiAT5-3 shows a complex phosphorylation pattern at its N-terminus and other phosphorylation sites could contribute to ApiAT5-3 regulation. Mimicking these conditions in a heterologous assay, or in parasites, without prior knowledge of the abundance of the phosphorylation on each of these residues becomes hard to interpret and should be the subject of further studies.

Apart from regulating amino acid transport, phosphorylation of transporters has also been shown to regulate trafficking to the surface (34–36). However, a role for S56 in trafficking is less likely for two reasons: i) we did not observe any obvious defects in surface translocation of the transporter in parasites and ii) *Tg*CDPK3 phosphorylates S56 shortly before, or during egress, at which state the transporter is already on the surface. If S56 phosphorylation was important for surface translocation, we would expect this to occur at an earlier stage. However, we cannot exclude the possibility that minor differences in trafficking capacity impact tyrosine transport, resulting in the growth phenotype.

Whatever the molecular explanation for the phenotype, it is evident that *Tg*CDPK3-mediated phosphorylation of ApiAT5-3 is important for parasite fitness.

Interestingly we haven't been able to rescue the effect of *apiAT5-3* loss in our conditional KO parasites through growth in high tyrosine concentrations. These

415 results differ from those in Parker, K., *et al* whereby growth can, at least partially,
416 be rescued in high tyrosine medium (19). One mechanism to counter low tyrosine
417 levels that most organisms possess, is the ability to convert phenylalanine into
418 tyrosine, via the enzyme phenylalanine-4-hydroxylase (AAH). However, the lack of
419 tyrosine import in ApiAT5-3 conditional KO's cannot be overcome in the presence
420 of high levels of phenylalanine, indicating that this pathway is not available.
421 Indeed, both isoforms of AAH (AAH1 and AAH2) have recently been shown to be
422 secreted into the host cell during *Toxoplasma* infection, where they would be
423 unable to rescue a tyrosine transporter defect in the plasma membrane (33,37).
424 Another explanation as to why Parker, K., *et al.* have successfully rescued the
425 effects of *apiAP5-3* deletion through addition of excess tyrosine, could be via the
426 upregulation of alternative transporters. Although a small amount of tyrosine
427 appears to be imported in our *apiAT5-3* KO line (Fig. 5B), this is likely due to the
428 presence of residual ApiAT5-3 protein in the plasma membrane after RAP-
429 treatment. Along with our inability to rescue growth upon tyrosine
430 supplementation, we conclude that this residual tyrosine import is unlikely due to
431 an alternative transporter. Further to this, our transcriptomic analysis argues
432 against a rapid sensing and transcriptional compensation for the lack of tyrosine
433 import, so if upregulation of alternative transporters occurs, it will be a slow
434 process. Another explanation may be that slight differences in the genetic
435 background or passage history, and potential epigenetic changes in the parental
436 strains, leads to a difference in capacity for amino acid transport. There is some
437 indication that this may be the case as, in our metabolomics experiments, the
438 ApiAT5-3 deletion showed reduced levels of glycine and aspartic acid in addition
439 to tyrosine, while in Parker et al., other amino acids where observed to be less

abundant in addition to tyrosine. We also saw an increase in abundance of some amino acids that differ from Parker, K *et al.* It may be interesting in the future, to compare our *apiAT5-3* KO with that of Parker, K., *et al.* and identify any compensatory mechanisms the parasites can use to adjust to tyrosine starvation. Interestingly, deletion of *apiAT5-3* leads to a growth arrest that is not accompanied by major transcriptional responses. This is reminiscent of the hibernation state in *Plasmodium falciparum*, whereby depletion of isoleucine, an essential amino acid for this parasite, leads to arrest in growth without a major stress response (38). This would suggest that translational arrest may be a common response among apicomplexan parasites during amino acid starvation.

In summary we show that ApiAT5-3, a novel *T. gondii* tyrosine transporter, is rapidly phosphorylated in a *Tg*CDPK3 dependent manner at S56 prior to, and during egress from the host cell. The phosphorylation of S56 appears important for parasite fitness. These results, together with previous studies, support the notion that *Tg*CDPK3 simultaneously targets several proteins in, or at, the plasma membrane, controlling very divergent biological processes, such as motility and metabolism. The phenotypes observed in Δ*cdpk3* parasites may therefore be an accumulation of effects on various proteins, which is likely true for other kinases as well.

Materials and Methods

Parasite culture

T. gondii parasites were cultured in a confluent monolayer of human foreskin fibroblasts (HFFs) maintained in Dulbecco's Modified Eagle Medium (DMEM), GlutaMAX supplemented with 10% foetal bovine serum, at 37°C and 5% CO_2.

Plasmid and parasite strain generation

A comprehensive list of primers and parasite lines used throughout this study are described in S1 and S2 Tables respectively. To generate the epitope tagged ApiAT5-3::HA line, the *apiAT5-3* gene and associated 5' UTR were PCR-amplified from RH *T. gondii* gDNA using the primers 1 and 2 and cloned using Gibson assembly (39) into pGRA::HA::HPT (40), linearised with HindIII and NcoI. 25 µg of the pGRA::ApiAT5-3::HA vector was transfected into RH *Δhxgprt* parasites as previously described (41). 16-20 hrs after transfection, transgenic parasites were selected using 25 µM mycophenolic acid (MPA) and 50 µg/ml xanthine (XAN). To generate the ApiAT5-3_loxP conditional KO lines, the *apiAT5-3* 5'UTR was first PCR-amplified from gDNA with primers 3 and 4. This PCR product was inserted, along with the synthetic DNA constructs *loxP_apiAT5-3_loxP_yfp* and *loxP*(-100)*_apiAT5-3* (see S1 Table for full sequences), by Gibson assembly into pG140::Actin::YFP (42) that had been PCR-amplified using primers 5 and 6 to remove the actin gene. 2 µg of the subsequent pG140::ApiAT5-3_loxP::YFP plasmid was linearised with ScaI and co-transfected into RH *Δku80Δhxgprt* with pSag1::Cas9-U6::dbl-sgApiAT5-3, in a molar ratio of 1:10. The pSag1::Cas9-U6::dbl-sgApiAT5-3 vector was generated by PCR-amplification of the

485 pSag1::Cas9-U6 (43) vector using primers 7 and 8 to insert the 5' gRNA (gRNA 1)
486 and 9 and 8 to insert the 3' gRNA (gRNA 2), prior to re-ligation with T4 DNA Ligase
487 (New England Biolabs M0202). gRNA 1 was then amplified using primers 10 and
488 11 and Gibson cloned into the pSag1::Cas9-U6::sg2ApiAT5-3 that had been
489 linearised with KpnI and XhoI as per (25). Transgenic parasites were selected
490 using MPA/XAN as described for pGRA::ApiAT5-3::HA. 5' and 3' integration was
491 confirmed using primer pairs 12 and 13, and 14 and 15 respectively. Absence of
492 WT *apiAT5-3* was confirmed using primers 16 and 17. DiCre-mediated *apiAT5-3*
493 excision was induced with the addition of 50 nM RAP to ApiAT5-3_loxP parasites
494 for 4 hrs. Excision was confirmed using primers 13 and 16. To introduce an ectopic
495 copy of *apiAT5-3* into the *uprt* gene locus, the *apiAT5-3* gene, and associated 5'
496 UTR, were PCR-amplified from gDNA using primers 18 and 19 which was then
497 inserted into the BamHI/ PacI digested pUPRT::DHFR-D vector (Addgene plasmid
498 #58258 (43)) using Gibson assembly. To generate the pUPRT::ApiAT5-
499 3_S56A::HA and pUPRT::ApiAT5-3_S56D::HA vectors, the pUPRT::ApiAT5-3::HA
500 vector was modified by site directed mutagenesis using the primers 20 and 21
501 (S56A) or 22 (S56D). pUPRT::ApiAT5-3::HA, pUPRT::ApiAT5-3_S56A::HA and
502 pUPRT::ApiAT5-3_S56D::HA were linearised with PciI prior to the co-transfection
503 of 2 µg into RH *Δku80Δhxgprt* ApiAT5-3_loxP with pSag1::Cas9-U6::sgUPRT
504 (Addgene 54467 (43)) in a molar ratio of 1:10. Transgenic parasites were selected
505 by the addition of 5 µM 5'-fluo-2'-deoxyuridine to culture medium, 16-20 hrs post-
506 transfection. Integration into the genome was confirmed using primer pairs 24
507 and 25, and 26 and 27 respectively. Absence of *uprt* was confirmed using primers
508 28 and 29.
509

510 **Western blotting and immunofluorescent imaging**

511 For Western blot analysis, intracellular parasites were lysed in Laemmli buffer (60
512 mM Tris-HCl pH6.8, 1% SDS, 5% glycerol, 5% b-mercaptoethanol, 0.01%
513 bromophenol blue) and heated to 37°C for 30 mins prior to separation on a 10%
514 sodium dodecyl-polyacrylamide gel. Proteins were transferred onto a
515 nitrocellulose membrane prior to blocking in 3% milk, 0.1% Tween-20 PBS. HA-
516 tagged ApiAT5-3 was detected using rat anti-HA (1:500), followed by goat anti-rat
517 horseradish peroxidase-conjugated secondary antibody (1:2500).
518 IFA's were performed on intracellular parasites grown in HFFs on glass coverslips.
519 1×10^5 parasites were seeded 24 hrs prior to fixation with 3% formaldehyde (FA).
520 PBS 0.1% Triton X-100 was added to the fixed cells for 10 mins prior to blocking
521 with 3% bovine serum albumin in PBS for 1 hr. ApiAT5-3::HA was visualised using
522 rat anti-HA (1:500) followed by addition of Alexa488 conjugated donkey anti-rat
523 secondary antibody (1:2000) and DAPI, 5 μg/ml.

524 **Plaque assay and amino acid complementation**

525 For plaque assay analysis, 150 parasites were seeded on confluent HFF
526 monolayers, grown in 24-well plates, and left undisturbed for 5 days, before fixing
527 with chilled methanol and staining with 0.1% crystal violet. To assess growth in
528 excess tyrosine, plaque assays were repeated either at normal tyrosine levels (400
529 μM L-tyrosine disodium salt; as per Gibco manufacturer) or in DMEM
530 supplemented with 2mM L-tyrosine disodium salt (dissolved for 1 hour at 50 °C).
531 To ensure tyrosine had successfully dissolved samples of the media were analysed
532 by GC-MS as previously described (18).

533 **Replication assay**

534 2×10^4 ApiAT5-3_loxP parasites were seeded in triplicate on confluent HFFs in
535 both culture flasks and glass bottom 8-well imaging plates and left to invade for 1
536 hour prior to treatment with 50 nM RAP or equivalent volume DMSO, for 4 hrs.
537 Parasites were imaged at 24, 36 and/or 48 hrs and split at 36 hrs into new flasks
538 and imaging wells for the subsequent replication cycle. At each time point
539 parasites were fixed in 3% FA and imaged on a Nikon Eclipse Ti-U inverted
540 fluorescent microscope. Parasites/vacuole were counted manually from 5 fields
541 of view at 20× magnification using the Nikon NIS-Elements software.

542

543 **Live cell microscopy**

544 ApiAT5-3_loxP parasites were treated with RAP or DMSO as previously described.
545 36 hrs into cycle 2 post RAP-treatment parasites were syringe lysed and seeded
546 in glass bottom, 8-well imaging plates in a 1:1 ratio with RH Tom parasites. After
547 a further 29 hrs, live parasites were imaged on a Nikon Eclipse Ti-U inverted
548 fluorescent microscope every 30 mins for the next 30 hrs, in a temperature-
549 controlled chamber at 37 °C and 5% CO_2. Images were analysed using the Nikon
550 NIS-Elements software.

551

552 **Ionophore induced egress and death assays**

553 ApiAT5-3_loxP parasites were seeded in 96-well imaging plates at a MOI of 0.5, 36
554 hrs post RAP/DMSO-treatment. Ionophore induced egress assays were performed
555 in triplicate at 37 °C in Ringers buffer (155 mM NaCl, 3 mM KCl, 2 mM $CaCl_2$, 1 mM
556 $MgCl_2$, 3 mM NaH_2PO_4, 10 mM HEPES, 10 mM glucose) 30 hrs later. The parasites

were incubated with 8 µM Ca^{2+} ionophore A23187 for 0, 0.5, 1, 1.5, 2, 2.5, 3, 3.5, 4 and 5 mins prior to the addition of 16% FA to a final concentration of 3% for 15 mins. Wells were subsequently washed with PBS and stained with 5 µg/ml DAPI. Automated image acquisition of 25 fields per well was performed on a Cellomics Array Scan VTI HCS reader (Thermo Scientific) using a 20× objective. Image analysis was performed using the Compartmental Analysis BioApplication on HCS Studio (Thermo Scientific).

Competition assays and flow cytometry

5×10^6 ApiAT5-3$^{ApiAT5\text{-}3}$, ApiAT5-3$^{ApiAT5\text{-}3_S56A}$ and ApiAT5-3$^{ApiAT5\text{-}3_S56D}$ parasites were mixed in a 1:1 ratio with Δ*apiAT5-3*$^{ApiAT5\text{-}3}$, Δ*apiAT5-3*$^{ApiAT5\text{-}3\_S56A}$ and Δ*apiAT5-3*$^{ApiAT5\text{-}3\_S56D}$ respectively. 5×10^4 parasites were added to fresh HFF monolayers before spinning the rest of the sample at 72 × g to remove host cell debris for 1 min. The supernatant was spun at 2049 × g for 5 mins. The pellet was fixed for 10 mins in 3% FA, washed in PBS and stained with 5 µg/ml DAPI. The sample was washed and resuspended in PBS before running on a flow cytometer. All parasites were gated on DAPI fluorescence to prevent results being skewed by remaining unstained host cell debris. The proportion of DAPI (+); YFP (+) (representing Δ*apiAT5-3*$^{ApiAT5\text{-}3/S56A/S56D}$) compared to DAPI (+); YFP (-) (representing ApiAT5-3$^{ApiAT5\text{-}3/S56A/S56D}$) was calculated. The process was repeated 14 days later for comparison to day 0.

Oocyte maintenance and radiotracer uptake assays

ApiAT5-3, ApiAT5-3_S56A and ApiAT5-3_S56D were PCR amplified from Δ*apiAT5-3*$^{\text{ApiAT5-3}}$, Δ*apiAT5-3*$^{\text{ApiAT5-3\_S56A}}$ and Δ*apiAT5-3*$^{\text{ApiAT5-3\_S56D}}$ cDNA, respectively, using primers 30 and 31 to add a region of homology to the XkbN plasmid at the 5' end and a HA tag to the 3' end of each gene. These fragments were then amplified with primers 32 and 33 to add a 3' XkbN homology overhang. These resulting fragments were inserted by Gibson assembly into the XkbN1_*Pf*HT (a version of pSPGT1 (44) with a NotI site added to the MCS, provided by Ksenija Slavic) which had been digested with BglII and NotI, to remove the *Pf*HT gene. The resulting XkbN_ApiAT5-3, XkbN_ApiAT5-3_S56A and XkbN_ApiAT5-3 _S56D plasmids were linearised with XbaI for in vitro transcription using the Thermo Fisher mMessage mMachine transcription kit. Stage V to VI defolliculated *X. laevis* oocytes were obtained commercially (Ecocyte Biosciences) for subsequent functional transport studies. Oocytes were microinjected with cRNA (20 to 40 ng in 30 nl of water) encoding *apiAT5-3* template or with a comparable amount of diethylpyrocarbonate-treated water. The oocytes were maintained at 18 °C in oocyte Ringer 2 buffer (82.5 mM NaCl, 2.5 mM KCl, 1.5 mM $CaCl_2$, 1mM Na_2HPO_4, 1 mM $MgCl_2$ and 5 mM HEPES) and used for transport studies 72 hrs after cRNA injection. Transport measurements were performed at room temperature on groups of 10 oocytes in ND96 medium (96 mM NaCl, 2 mM KCl, 2 mM $CaCl_2$, 1 mM $MgCl_2$ and 5 mM HEPES) containing 1 µM radiolabelled U-^{14}C-L-tyrosine (specific activity of 486 mCi/mmol; Perkin Elmer), U-^{14}C-L-phenylalanine (specific activity of 508 mCi/mmol; Perkin Elmer) or U-^{14}C-L-valine (specific activity of 271 mCi/mmol; Perkin Elmer). Transport was measured at 10 min, over which time

603 uptake of L-tyrosine is linear (19). Each result was confirmed by at least 3
604 independent experiments.
605

606 **Metabolite labelling and extraction**

607 ApiAT5-3_loxP, Δ*apiAT5-3*$^{\text{ApiAT5-3}}$, Δ*apiAT5-3*$^{\text{ApiAT5-3\_S56A}}$ and Δ*apiAT5-3*$^{\text{ApiAT5-3\_S56D}}$
608 parasites were treated in triplicate with 50 nM RAP and, at the end of the first
609 cycle, seeded in 15 cm culture flasks. Stable isotope labelling (1 hr) of extracellular
610 parasites with 0.8 mM U-^{13}C-L-tyrosine or 4 mM U-^{13}C-L-isoleucine, metabolite
611 extraction and subsequent GC-MS analysis were all performed as per (18), on an
612 Agilent GC-MSD (7890B-5977A). Data analysis was carried out using GAVIN
613 software (45).

614 **RNA sequencing analysis**

615 *T. gondii* RNA was extracted as per the Qiagen RNA-easy mini kit user handbook
616 (#74104) from ~5×10^6 ApiAT5-3_loxP or ApiAT5-3_loxP$^{\text{dDiCre}}$ parasites at 0, 4 and
617 60 hrs post RAP-treatment. Analysis was performed in triplicate. The FASTQ files
618 were aligned using Bowtie 2 (46) to Ensembl Protist's release 35 of *T. gondii*
619 (ToxoDB-7.1). They were then quantified using RSEM before being processed
620 using Bioconducor (47). We used DESeq2 (48) to account for gene length and
621 library size, and to test for the interaction between treatment and time point to
622 generate the differential genelist. We corrected for multiple testing using the
623 Benjamini-Hochberg procedure for false discovery rates. To validate the
624 recodonised transcript, we both re-aligned to a custom genome rebuilt to include
625 the novel sequence, and also used a pseudo-alignment approach to quantify purely
626 the reads associated with the novel sequence (49).

627

628 Acknowledgements

629 We thank all members of the Treeck laboratory for critical discussions. We thank
630 Giel Van Dooren and Sebastian Lourido for sharing unpublished data. We thank
631 members of the following Science Technology platforms at the Francis Crick
632 Institute: Bioinformatics, Advanced Sequencing, Peptide Synthesis, Proteomics
633 and Flow Cytometry.

634

635 References

636 1. Lourido S, Moreno SN. The calcium signaling toolkit of the Apicomplexan
637 parasites Toxoplasma gondii and Plasmodium spp. Cell calcium. 2015
638 Mar;57(3):186–93.

639 2. Sidik SM, Hortua Triana MA, Paul AS, El Bakkouri M, Hackett CG, Tran F, et al.
640 Using a Genetically Encoded Sensor to Identify Inhibitors of Toxoplasma gondii
641 Ca2+ Signalling. The Journal of biological chemistry. 2016 Mar 1;

642 3. Stewart RJ, Whitehead L, Nijagal B, Sleebs BE, Lessene G, McConville MJ, et al.
643 Analysis of Ca2+ mediated signalling regulating Toxoplasma infectivity reveals
644 complex relationships between key molecules. Cellular microbiology. 2016 Oct
645 26;

646 4. Carruthers VB, Sibley LD. Mobilization of intracellular calcium stimulates
647 microneme discharge in Toxoplasma gondii. Molecular microbiology. 1999
648 Jan;31(2):421–8.

649 5. Wetzel DM, Chen LA, Ruiz FA, Moreno SN, Sibley LD. Calcium-mediated
650 protein secretion potentiates motility in Toxoplasma gondii. Journal of cell
651 science. 2004 Nov 15;117(Pt 24):5739–48.

652 6. Endo T, Sethi KK, Piekarski G. Toxoplasma gondii: calcium ionophore A23187-
653 mediated exit of trophozoites from infected murine macrophages. Experimental
654 parasitology. 1982 Apr;53(2):179–88.

655 7. Lovett JL, Sibley LD. Intracellular calcium stores in Toxoplasma gondii govern
656 invasion of host cells. Journal of Cell Science. 2003 Jul 15;116(14):3009–16.

8. Mondragon R, Frixione E. Ca(2+)-dependence of conoid extrusion in Toxoplasma gondii tachyzoites. The Journal of eukaryotic microbiology. 1996 Mar;43(2):120–7.

9. Black MW, Arrizabalaga G, Boothroyd JC. Ionophore-resistant mutants of Toxoplasma gondii reveal host cell permeabilization as an early event in egress. Molecular and Cellular Biology. 2000 Dec;20(24):9399–408.

10. Moudy R, Manning TJ, Beckers CJ. The loss of cytoplasmic potassium upon host cell breakdown triggers egress of Toxoplasma gondii. Journal of Biological Chemistry. 2001 Nov 2;276(44):41492–501.

11. McCoy JM, Whitehead L, van Dooren GG, Tonkin CJ. TgCDPK3 regulates calcium-dependent egress of Toxoplasma gondii from host cells. PLoS pathogens. 2012;8(12):e1003066.

12. Lourido S, Tang K, Sibley LD. Distinct signalling pathways control Toxoplasma egress and host-cell invasion. The EMBO journal. 2012 Dec 12;31(24):4524–34.

13. Garrison E, Treeck M, Ehret E, Butz H, Garbuz T, Oswald BP, et al. A Forward Genetic Screen Reveals that Calcium-dependent Protein Kinase 3 Regulates Egress in Toxoplasma. Plos Pathogens [Internet]. 2012 Nov;8(11). Available from: ://WOS:000311997100060

14. Huang JF, Teyton L, Harper JF. Activation of a Ca2+-dependent protein kinase involves intramolecular binding of a calmodulin-like regulatory domain. Biochemistry. 1996;35(40):13222–30.

15. Wernimont AK, Amani M, Qiu W, Pizarro JC, Artz JD, Lin YH, et al. Structures of parasitic CDPK domains point to a common mechanism of activation. Proteins. 2011 Mar;79(3):803–20.

16. Wernimont AK, Artz JD, Finerty P Jr, Lin YH, Amani M, Allali-Hassani A, et al. Structures of apicomplexan calcium-dependent protein kinases reveal mechanism of activation by calcium. Nature structural & molecular biology. 2010 May;17(5):596–601.

17. Treeck M, Sanders JL, Gaji RY, LaFavers KA, Child MA, Arrizabalaga G, et al. The Calcium-Dependent Protein Kinase 3 of Toxoplasma Influences Basal Calcium Levels and Functions beyond Egress as Revealed by Quantitative Phosphoproteome Analysis. Plos Pathogens [Internet]. 2014 Jun;10(6). Available from: ://WOS:000338197400032

18. MacRae JI, Sheiner L, Nahid A, Tonkin C, Striepen B, McConville MJ. Mitochondrial Metabolism of Glucose and Glutamine Is Required for Intracellular Growth of Toxoplasma gondii. Cell Host & Microbe. 2012 Nov 15;12(5):682–92.

19. Parker KER, Fairweather SJ, Rajendran E, Blume M, McConville MJ, Broer S, et al. Characterization of the apicomplexan amino acid transporter (ApiAT) family in Toxoplasma gondii. bioRxiv. 2018 Apr 26;306993.

20. Hofmann. TMbase - A database of membrane spanning proteins segments. Biol Chem Hoppe-Seyler [Internet]. 1993 [cited 2018 May 25];374(166). Available from: http://www.ch.embnet.org/documentation/mfc-35.pdf

21. Thompson A, Schäfer J, Kuhn K, Kienle S, Schwarz J, Schmidt G, et al. Tandem Mass Tags: A Novel Quantification Strategy for Comparative Analysis of Complex Protein Mixtures by MS/MS. Analytical Chemistry. 2003 Apr;75(8):1895–904.

22. Nebl T, Prieto JH, Kapp E, Smith BJ, Williams MJ, Yates 3rd JR, et al. Quantitative in vivo Analyses Reveal Calcium-dependent Phosphorylation Sites and Identifies a Novel Component of the Toxoplasma Invasion Motor Complex. PLOS Pathogens. 2011 Sep 29;7(9):e1002222.

23. Lourido S, Jeschke GR, Turk BE, Sibley LD. Exploiting the Unique ATP-Binding Pocket of Toxoplasma Calcium-Dependent Protein Kinase 1 To Identify Its Substrates. Acs Chemical Biology. 2013 Jun;8(6):1155–62.

24. Sidik SM, Huet D, Ganesan SM, Huynh M-H, Wang T, Nasamu AS, et al. A Genome-Wide CRISPR Screen in Toxoplasma Identifies Essential Apicomplexan Genes. Cell. 2016 Sep 8;166(6):1423-1435.e12.

25. Long S, Wang Q, Sibley LD. Analysis of non-canonical calcium dependent protein kinases in Toxoplasma gondii by targeted gene deletion using CRISPR/Cas9. Infection and immunity. 2016 Jan 11;

26. Gaji RY, Johnson DE, Treeck M, Wang M, Hudmon A, Arrizabalaga G. Phosphorylation of a Myosin Motor by TgCDPK3 Facilitates Rapid Initiation of Motility during Toxoplasma gondii egress. PLoS pathogens. 2015 Nov;11(11):e1005268.

27. Liu K-H, Tsay Y-F. Switching between the two action modes of the dual-affinity nitrate transporter CHL1 by phosphorylation. The EMBO Journal. 2003 received;22(5):1005–13.

28. Jang H-Y, Rhee J, Carlson JE, Ahn S-J. The Camelina aquaporin CsPIP2;1 is regulated by phosphorylation at Ser273, but not at Ser277, of the C-terminus and is involved in salt- and drought-stress responses. Journal of Plant Physiology. 2014 Sep 15;171(15):1401–12.

29. Lee SC, Lan W-Z, Kim B-G, Li L, Cheong YH, Pandey GK, et al. A protein phosphorylation/dephosphorylation network regulates a plant potassium channel. PNAS. 2007 Oct 2;104(40):15959–64.

30. Tamura N, Oku M, Ito M, Noda NN, Inagaki F, Sakai Y. Atg18 phosphoregulation controls organellar dynamics by modulating its phosphoinositide-binding activity. J Cell Biol. 2013 Aug 19;202(4):685–98.

31. Ramamoorthy S, Shippenberg TS, Jayanthi LD. Regulation of Monoamine Transporters: Role of Transporter Phosphorylation. Pharmacology & therapeutics. 10;129(2):220–38.

736 32. Aryal B, Laurent C, Geisler M. Learning from each other: ABC transporter
737 regulation by protein phosphorylation in plant and mammalian systems.
738 Biochemical Society Transactions. 2015 Oct 1;43(5):966–74.

739 33. Marino ND, Boothroyd JC. Toxoplasma growth in vitro is dependent on
740 exogenous tyrosine and is independent of AAH2 even in tyrosine-limiting
741 conditions. Exp Parasitol. 2017 Feb 28;

742 34. Abramian AM, Comenencia-Ortiz E, Modgil A, Vien TN, Nakamura Y, Moore
743 YE, et al. Neurosteroids promote phosphorylation and membrane insertion of
744 extrasynaptic GABAA receptors. PNAS. 2014 May 13;111(19):7132–7.

745 35. Rice WL, Zhang Y, Chen Y, Matsuzaki T, Brown D, Lu HAJ. Differential,
746 Phosphorylation Dependent Trafficking of AQP2 in LLC-PK1 Cells. Rappoport
747 JZ, editor. PLoS ONE. 2012 Feb 28;7(2):e32843.

748 36. Nissen-Meyer LSH, Popescu MC, Hamdani EH, Chaudhry FA. Protein Kinase C-
749 Mediated Phosphorylation of a Single Serine Residue on the Rat Glial Glutamine
750 Transporter SN1 Governs Its Membrane Trafficking. J Neurosci. 2011 Apr
751 27;31(17):6565–75.

752 37. Wang ZT, Verma SK, Dubey JP, Sibley LD. The aromatic amino acid
753 hydroxylase genes AAH1 and AAH2 in Toxoplasma gondii contribute to
754 transmission in the cat. PLOS Pathogens. 2017 Mar 13;13(3):e1006272.

755 38. Babbitt SE, Altenhofen L, Cobbold SA, Istvan ES, Fennell C, Doerig C, et al.
756 Plasmodium falciparum responds to amino acid starvation by entering into a
757 hibernatory state. PNAS. 2012 Nov 20;109(47):E3278–87.

758 39. Gibson DG, Benders GA, Andrews-Pfannkoch C, Denisova EA, Baden-Tillson H,
759 Zaveri J, et al. Complete chemical synthesis, assembly, and cloning of a
760 Mycoplasma genitalium genome. Science. 2008 Feb 29;319(5867):1215–20.

761 40. Saeij JPJ, Boyle JP, Coller S, Taylor S, Sibley LD, Brooke-Powell ET, et al.
762 Polymorphic Secreted Kinases Are Key Virulence Factors in Toxoplasmosis.
763 Science. 2006 Dec 15;314(5806):1780–3.

764 41. Soldati D, Boothroyd JC. Transient transfection and expression in the obligate
765 intracellular parasite Toxoplasma gondii. Science. 1993 Apr 16;260(5106):349–
766 52.

767 42. Andenmatten N, Egarter S, Jackson AJ, Jullien N, Herman J-P, Meissner M.
768 Conditional genome engineering in Toxoplasma gondii uncovers alternative
769 invasion mechanisms. Nature Methods. 2013 Feb;10(2):125–7.

770 43. Shen B, Brown KM, Lee TD, Sibley LD. Efficient gene disruption in diverse
771 strains of Toxoplasma gondii using CRISPR/CAS9. mBio. 2014;5(3):e01114-14.

772 44. Woodrow CJ, Penny JI, Krishna S. Intraerythrocytic Plasmodium falciparum
773 expresses a high affinity facilitative hexose transporter. J Biol Chem. 1999 Mar
774 12;274(11):7272–7.

775 45. Behrends V, Tredwell GD, Bundy JG. A software complement to AMDIS for
776 processing GC-MS metabolomic data. Anal Biochem. 2011 Aug 15;415(2):206–
777 8.

778 46. Langmead B, Salzberg SL. Fast gapped-read alignment with Bowtie 2. Nat Meth.
779 2012 print;9:357–9.

780 47. Huber W, Carey VJ, Gentleman R, Anders S, Carlson M, Carvalho BS, et al.
781 Orchestrating high-throughput genomic analysis with Bioconductor. Nat
782 Methods. 2015 Feb;12:115–21.

783 48. Love MI, Huber W, Anders S. Moderated estimation of fold change and
784 dispersion for RNA-seq data with DESeq2. Genome Biology. 2014;15:1–21.

785 49. Bray NL, Pimentel H, Melsted P, Pachter L. Near-optimal probabilistic RNA-seq
786 quantification. Nat Biotechnol. 2016 May;34:525–7.

787

788

Figure Legends

Fig 1. ApiATP5-3 localises to the plasma membrane and is phosphorylated at serine 56 upon ionophore treatment

(A) Topology prediction of ApiAT5-3. Serine 56 is predicted to be located on the luminal side of the parasite **(B)** Quantification of the phosphorylation state of residues in the ApiAT5-3 N-terminus in *TgCDPK3* KOs and during ionophore-induced egress (from (17))**.** Upper panel: The heatmap shows differential phosphorylation of S56 in *Tg*CDPK3 mutants compared to WT parasites, but not any other of the identified phosphorylation sites. Intracellular (IC) and extracellular (EC) parasites with and without 1 µM ionophore (iono). P-site = phosphorylation site. Numbers represent residue position. Black 'x' = phosphorylation site not identified. Fold changes are $\log^2$. Bottom panel: Change in relative phosphorylation of ApiAT5-3 and proteins with previously described ionophore-dependent phosphorylation sites, measured after addition of 8 µM ionophore over 60 s. Numbers after the identifier represent the phosphorylation site quantified. **(C)** ApiAT5-3 was detected by Western blot analysis of ApiAT5-3::HA cell lysate using anti-HA antibody. **(D)** IFA of ApiAT5-3::HA expressing parasites shows that ApiAT5-3 localises to the periphery of the intracellular tachyzoite. Green = HA. Scale bar 10 µm.

Fig 2. ApiAT5-3 is essential for parasite proliferation

(A) Generation of the ApiAT5-3_loxP line using CRIPSPR/Cas9 to increase site-directed integration. Protospacer adjacent motif (PAM) indicated by black arrows. Primer pairs represented by coloured triangles. **(B)** Left panel: PCR analysis shows correct integration of the ApiAT5-3_loxP construct at both the 3' and 5'

ends and a loss of WT *apiAT5-3* at the endogenous locus. White * = non-specific bands. Right panel: Addition of RAP leads to correct recombination of the loxP sites. **(C)** Fluorescent microscopy of ApiAT5-3_loxP parasites 24 hrs after addition of DMSO or RAP. Scale bar 5 µm **(D)** Plaque assay showing loss of plaquing capacity of ApiAT5-3_loxP parasites upon RAP-treatment. **(E)** Parasite per vacuole number shown as mean %. n=3 **(F)** Stills from live video microscopy at 36, 42 and 45 hrs into 3rd lytic cycle post RAP-treatment. Red = RH Tom, dashed white line = WT ApiAT5-3_loxP, green = *apiAT5-3* KO. **(G)** Ionophore induced egress assay showing no significant difference between DMSO and RAP-treated ApiAT5-3_loxP (at 30 hrs into lytic cycle 2 post DMSO/RAP-treatment). Statistical analysis using multiple comparison 2-way ANOVA, n = 3.

Fig 3. Δ*apiAT5-3* parasites display a transcriptional response related to amino acid starvation

(A) Extracted reads for recodonised *apiAT5-3* from RNA sequence data show a significant reduction of *apiAT5-3* transcripts in RAP-treated ApiAT5-3_loxP lines 60 hrs post RAP-treatment compared to RAP-treated ApiAT5-3_loxP^{dDiCre} parasites. **(B)** Heatmap of genes that change significantly (adjusted p <0.05) in transcript read number between WT and Δ*apiAT5-3* 60 hrs post addition of RAP. **(C)** Gene ontology term enrichment shows that genes involved in translation processes are significantly enriched among the differentially expressed genes 60 hrs post RAP-treatment.

Fig 4. Δ*apiAT5-3*$^{ApiAT5-3\_S56A}$ demonstrates a fitness defect

(A) Generation of the ApiAT5-3$^{ApiAT5-3/_S56A/_S56D}$ complementation lines. PAM indicated by black arrow. Primer pairs represented by coloured triangles. **(B)** PCR analysis shows correct integration of the ApiAT5-3_loxP construct at both the 3' and 5' ends and a loss of *uprt*. White * = non-specific band **(C)** IFA of ApiAT5-3$^{ApiAT5-3/_S56A/_S56D_HA}$ expressing parasites shows that ApiAT5-3 is correctly trafficked to the periphery of the intracellular tachyzoite in both the presence (DMSO) and absence (Rapamycin) of the endogenous *apiAT5-3*. Red = HA. Green = YFP, indicating correct excision of the endogenous *apiAT5-3.* Scale bar 10 μm. **(D)** Growth competition assay by flow cytometry shows that Δ*apiAT5-3*$^{ApiAT5-3\_S56A}$ parasite growth is reduced relative to the non-excised ApiAT5-3$^{ApiAT5-3_S56A}$ line. Statistical analysis using multiple comparison, 2-way ANOVA of mean ratio to day 0 normalised to 1. ***p <0.001, n = 3.

Fig 5. Functional analysis of the ApiAT5-3 transporter

(A) *X. laevis* oocytes expressing ApiAT5-3 demonstrate a significant increase in ^{14}C-L-tyrosine uptake. 10 oocytes per experiment. Analysis carried out using a two-tailed, paired, Student's t-test. ***p <0.001 Box plots show mean, 1st and 3rd quartile and SD, n= 5. **(B)** Extracellular, RAP-treated, ApiAT5-3_loxP tachyzoites, labelled with ^{13}C-L-tyrosine or ^{13}C-L-isoleucine, display a marked decrease in tyrosine but not isoleucine import, relative to WT. n=2. **(C)** Plaque assay shows no rescue of growth of RAP-treated ApiAT5-3_loxP on addition of excess (2 mM) L-tyrosine. **(D)** *X. laevis* oocytes expressing *apiAT5-3_S56A* demonstrate a modest but insignificant reduction in ^{14}C-L-tyrosine uptake relative to *apiAT5-3* and *apiAT5-3_S56D*. 10 oocytes per experiment ****p <0.0001, ns = non-significant.

Analysis carried out using multiple comparison, one-way ANOVA. Box plots show mean, 1st and 3rd quartile and SD, n= 5.

Supporting information

S1 Fig. ApiAT5-3_loxP parasites that survive RAP-treatment retain the *apiAT5-3* gene.

PCR analysis using primers spanning the floxed *apiAT5-3* gene show that the small proportion of non-excised parasites present after RAP-treatment outgrow the excised Δ*apiAT5-3* parasites within 2 weeks.

S2 Fig. Verification of ApiAP5-3 complementation lines.

(A) Addition of RAP to the complemented parasite lines leads to correct recombination of the loxP sites and deletion of the endogenous *apiAT5-3* gene. **(B)** Plaque assay showing restoration of plaquing efficiency upon RAP-treatment of the ApiAT5-3_loxP line complemented with the WT or phosphomutant versions of the gene.

S3 Fig. Analysis of ApiAP5-3 transport function.

(A) *X. laevis* oocytes expressing *apiAT5-3* demonstrate an increase in ^{14}C-L-phenylalanine uptake but no significant ^{14}C-L-valine uptake. 10 oocytes per experiment. Analysis carried out using a two-tailed, paired, Student's t-test. *p <0.05, ns = non-significant. n= 2. **(B)** Relative abundance of amino acids in RAP-treated ApiAT5-3_loxP (KO) relative to Δ*apiATP5-3*$^{\text{ApiAT5-3}}$ (WT), shows that tyrosine is the most significantly reduced upon loss of ApiAT5-3. **(C)** Tyrosine

886 abundance in normal DMEM compared to DMEM supplemented with 2 mM
887 tyrosine.
888

889 **S1 Movie. Live video microscopy of Δ*apiAT5-3* parasites**

890 Live video microscopy of ApiAT5-3_loxP parasites 29 hrs into the 3rd lytic cycle
891 post DMSO- **(A)** or RAP- **(B)** treatment. Red = WT RH Tom, colourless parasites =
892 non-excised ApiAT5-3_loxP, green parasites = YFP expressing *apiAT5-3* KO.

893 **S1 Table. Primers and synthetic DNA sequences used throughout this study.**

894 **S2 Table. *Toxoplasma gondii* strains generated throughout this study.**

895 **S3 Table. RNA sequencing analysis of *apiAT5-3* conditional KO**

896 A list of all genes displaying $\log^2$ fold change in the RAP-treated Δ*apiAT5-3*$^{\text{ApiAT5-3}}$
897 compared to ApiAT5-3_loxP parasites, 4 and 60 hrs after RAP-treatment.
898

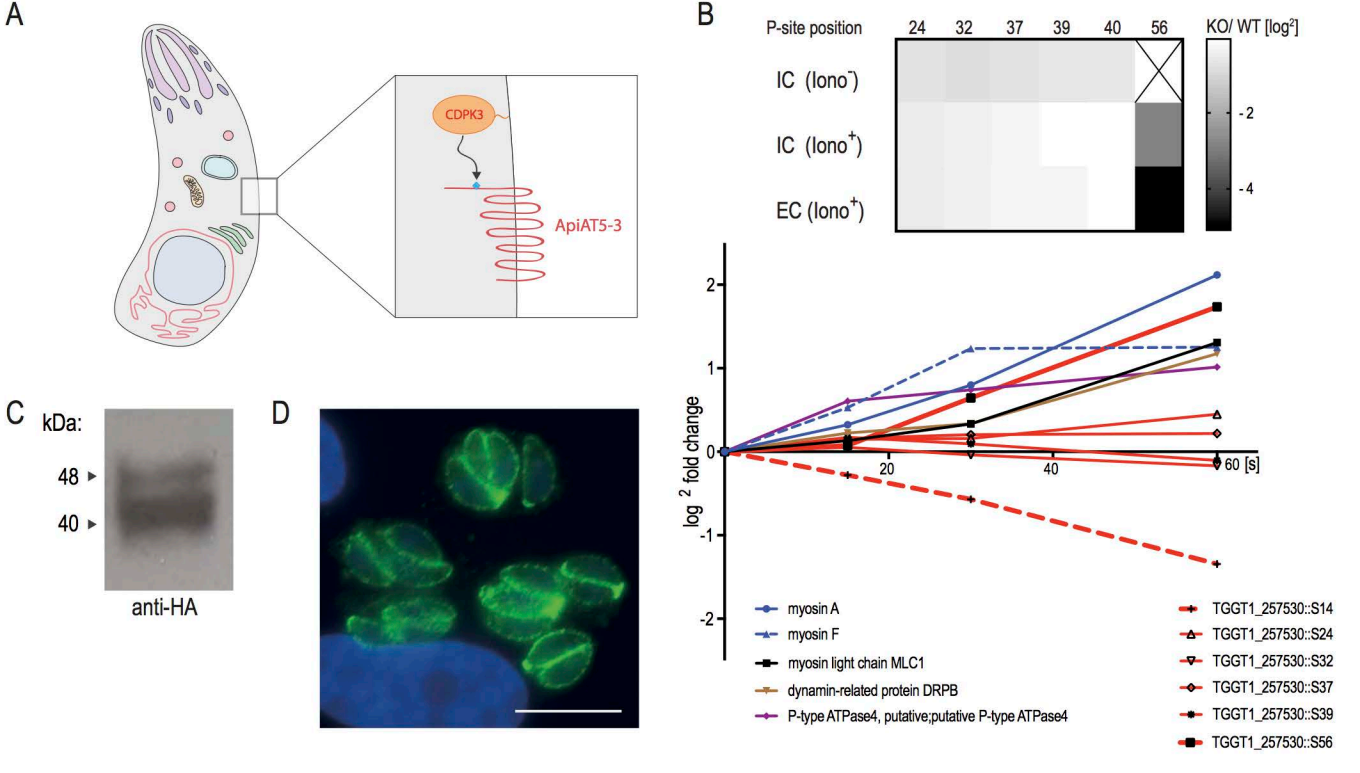
A
CDPK3
ApiAT5-3
B
P-site position
24
32
37
39
40
56
KO/ WT [log2]
IC (Iono-)
IC (Iono+)
EC (Iono+)
-2
-4
log 2 fold change
2
1
0
-1
-2
20
40
60 [s]
myosin A
myosin F
myosin light chain MLC1
dynamin-related protein DRPB
P-type ATPase4, putative;putative P-type ATPase4
TGGT1_257530::S14
TGGT1_257530::S24
TGGT1_257530::S32
TGGT1_257530::S37
TGGT1_257530::S39
TGGT1_257530::S56
C
kDa:
48
40
anti-HA
D

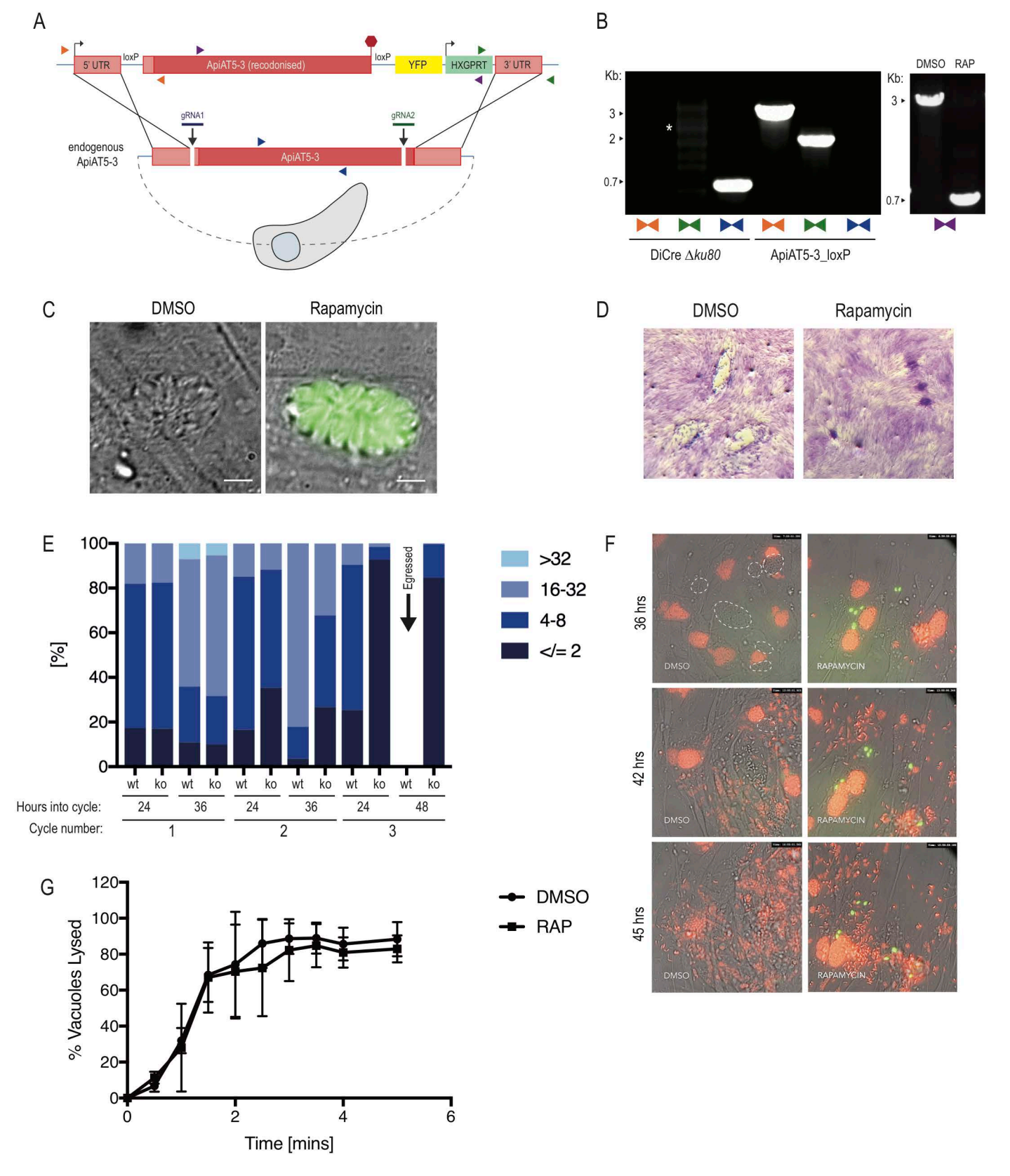
A
5' UTR
loxP
ApiAT5-3 (recodonised)
loxP
YFP
HXGPRT
3' UTR
gRNA1
gRNA2
endogenous ApiAT5-3
ApiAT5-3
B
Kb:
3
2
0.7
*
DiCre Δku80
ApiAT5-3_loxP
DMSO
RAP
Kb:
3
0.7
C
DMSO
Rapamycin
D
DMSO
Rapamycin
E
[%]
100
80
60
40
20
0
Egressed
>32
16-32
4-8
</= 2
wt ko wt ko wt ko wt ko wt ko wt ko
Hours into cycle:
24 36 24 36 24 48
Cycle number:
1 2 3
F
36 hrs
42 hrs
45 hrs
DMSO
RAPAMYCIN
G
% Vacuoles Lysed
120
100
80
60
40
20
0
0 2 4 6
Time [mins]
DMSO
RAP

A

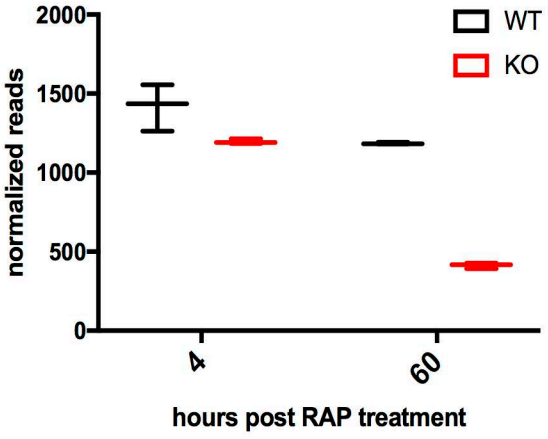

B

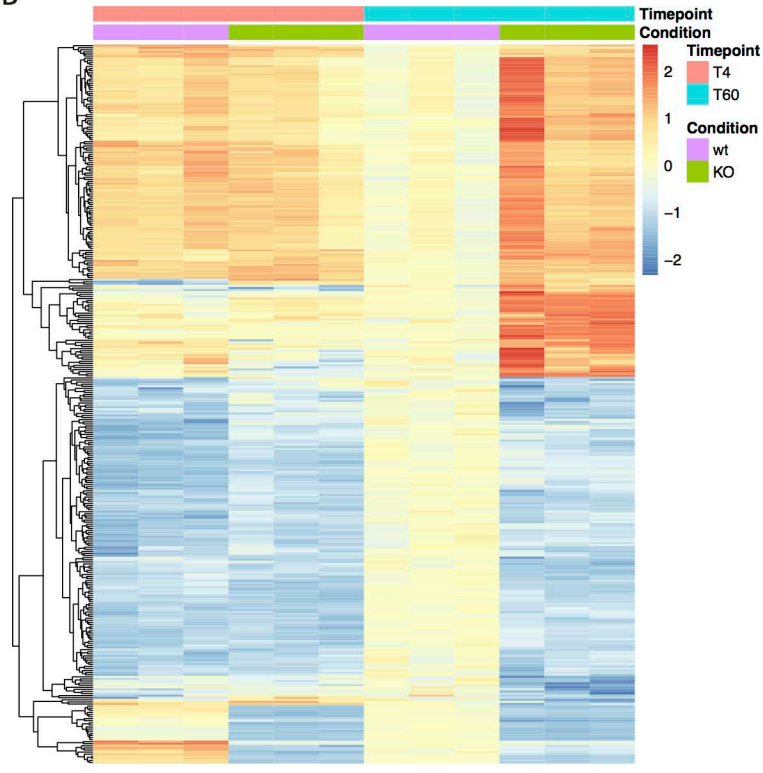

C

Biological process	Enrichment	Odds ratio	P-value	Benjamini	Bonferroni
translation	5.41	10.79	5.75E-38	1.38E-36	1.38E-36
biosynthetic process	2.65	4.06	2.28E-19	2.73E-18	5.46E-18
cellular nitrogen compound metabolic process	2.15	3.09	3.48E-14	2.78E-13	8.35E-13
biological process	1.26	1.93	1.77E-06	1.06E-05	4.25E-05
cellular protein modification process	1.42	1.52	4.60E-02	2.21E-01	1.00E+00

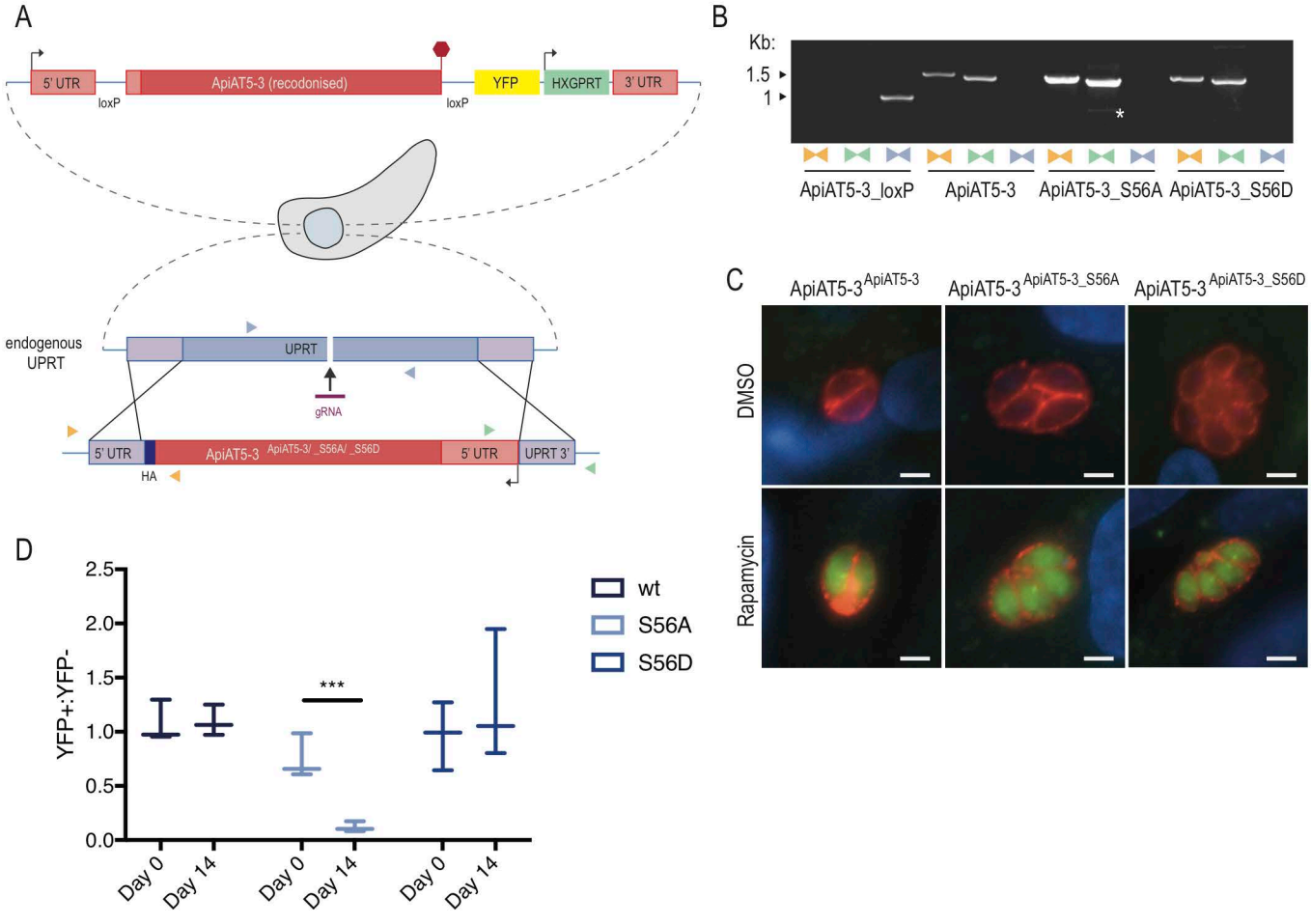
A
5' UTR
ApiAT5-3 (recodonised)
YFP
HXGPRT
3' UTR
loxP
loxP
endogenous UPRT
UPRT
gRNA
5' UTR
ApiAT5-3
ApiAT5-3/ _S56A/ _S56D
5' UTR
UPRT 3'
HA
B
Kb:
1.5
1
*
ApiAT5-3_loxP
ApiAT5-3
ApiAT5-3_S56A
ApiAT5-3_S56D
C
ApiAT5-3 ApiAT5-3
ApiAT5-3 ApiAT5-3_S56A
ApiAT5-3 ApiAT5-3_S56D
DMSO
Rapamycin
D
YFP+:YFP-
2.5
2.0
1.5
1.0
0.5
0.0
***
wt
S56A
S56D
Day 0
Day 14
Day 0
Day 14
Day 0
Day 14

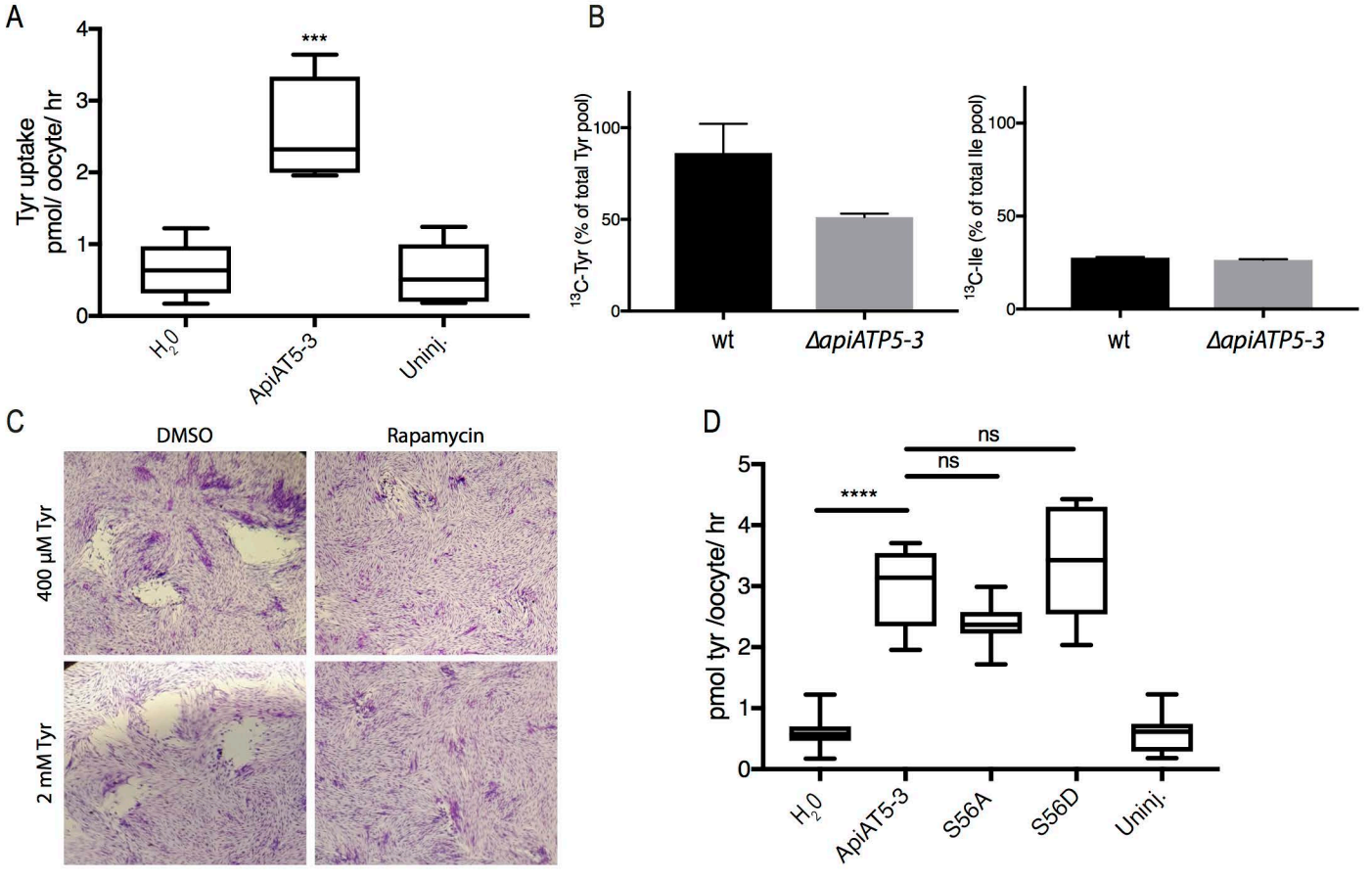
A
Tyr uptake pmol/ oocyte/ hr
***
H20
ApiAT5-3
Uninj.
B
13C-Tyr (% of total Tyr pool)
wt
ΔapiATP5-3
13C-Ile (% of total Ile pool)
wt
ΔapiATP5-3
C
DMSO
Rapamycin
400 µM Tyr
2 mM Tyr
D
pmol tyr /oocyte/ hr
ns
ns
****
H20
ApiAT5-3
S56A
S56D
Uninj.